The influence of Ti and Nb on solidification cracking of ferritic stainless steels, as determined using self-restrained samples

D. S. Konadu[1,2,*], P.G.H. Pistorius[1], M. Du Toit[3]

[1.] Department of Materials Science and Metallurgical Engineering, University of Pretoria, Pretoria 0002, South Africa.

[2.] Department of Materials Science and Engineering, University of Ghana, P. O. Box LG 77, Accra, Ghana.

[3.] School of Mechanical, Materials, Mechatronic and Biomedical Engineering, University of Wollongong, Australia

*Corresponding author

D. S. Konadu, email address: dskonadu@ug.edu.gh, Mobile No.: 00233-507230358

Abstract

The susceptibility to solidification cracking of ferritic stainless steels was studied using the self-restrained method. The unstabilised steel was compared with mono and dual stabilised (Ti and / or Nb) steels. Autogenous gas tungsten arc welding at a speed of 6 mm/s, 3 mm/s, and 1 mm/s was done. All the specimens cracked at a welding speed of 6 mm/s. The weld metal of both the unstabilised and the stabilised steels contained a mixture of columnar and equiaxed grains. At a welding speed of 3 mm/s, all the specimens except the unstabilised grade, cracked. The weld metal microstructures were mostly columnar and the dual stabilised grades showed equiaxed grains. At a welding speed of 1 mm/s, the Nb stabilised and the dual stabilised steel containing Mo cracked whilst the other alloys did not crack. At a welding speed of 1 mm/s, the weld metal was dominated by columnar grains. The cracks were interdendritic. The crack surfaces were enriched in Nb, Ti, Mn, Si, Al, Mn, and Mo. The unstabilised ferritic stainless steel was resistant to solidification cracking while the stabilised steels were not. Low melting point eutectic phases associated with Ti and Nb might have contributed to solidification cracking.

Keywords: Solidification cracking . Ferritic stainless steel . Microstructure . Gas tungsten arc welding.

1 Introduction

Ferritic stainless steels have ferrite as the dominant metallurgical phase and are used for their good resistance to stress corrosion cracking, pitting corrosion and crevice corrosion where moderate strength is required. Their applications are mostly in chemical plants, pulp and paper mills, refineries, automobile trim, catalytic converters and decorative purposes in general [1]. Ferritic stainless steels are a cheaper alternative to austenitic stainless steel because Ni is not added as an alloying element [1–5]. Ferritic stainless steels are generally more difficult to weld than austenitic stainless steels. This is mainly due to significant grain growth and the possible formation of martensite in the heat-affected zone (HAZ). The ferritic stainless steels are also susceptible to intergranular corrosion after welding due to sensitization [1]. Sensitization is the dropping of the grains due to the destruction of the grain boundaries. Chromium-rich carbides precipitate as $M_{23}C_6$ or M_7C_3 or M_6C. These carbides have a rich chromium content typically in the range of 42 to 65%, resulting in chromium depleted zones adjacent to the grain boundary precipitates. If the depletion is below 12 wt%, intergranular corrosion attack progresses along the chromium depleted grain boundaries since the corrosion resistance is significantly reduced. Thus, the grain boundaries are destroyed leading to sensitization [1, 3]. Sensitization can be prevented by reducing either the carbon and nitrogen amounts below certain levels or using titanium (Ti), niobium (Nb) or tantalum (Ta) as stabilizers [1,5-6]. Among the ferritic stainless steels, type AISI 430 is not stabilised, AISI 441 is dual stabilised (Ti and Nb), AISI 444 is dual stabilised (Ti and Nb) and contains Mo, AISI 436 and 439 are Nb and Ti mono stabilised respectively [7]. Lippold & Kotecki [1] states that the additions of Ti and Nb, and high impurity levels in ferritic stainless steels can decrease resistance to solidification cracking susceptibility. This is due to the solute elements segregating to grain boundaries to form low melting point phases.

Solidification cracking occurs in the fusion zone during the last stage of weld solidification, when the strength of the almost completely solidified weld is lower than the tensile stresses developed across the adjacent grains leading to cracking in the weld metal [3,5,8-9]. During the initial stage of solidification, a region known as the mushy zone exists. In this region, the solidification cells and dendrites have enough liquid for ‘healing’, making solidification cracking unlikely. In solidification studies, the mushy zone is the region where solid and liquid is

present at the same position. With further cooling, a rigid network is formed as solids begin to interact with each other. Strain accumulates with further bridging of solids leading to solidification cracking [5-6]. High welding speeds produce columnar grains which impinge at the weld centre and can cause solidification cracking [5-6,10]. Research on the solidification cracking of stainless steels has been largely limited to duplex and austenitic stainless steels [11–13]. The research of welding ferritic stainless steels has focused on the mechanical properties and the microstructure of the welded steel [14-15]. Kah and Dickinson [16] reported on the weldability of ferritic stainless steels using type AISI 430 and 444L materials. It was concluded that the hot cracking susceptibility of these materials was at least partially dependent on the composition and were promoted by sulphur, carbon, nitrogen, niobium, titanium, phosphorus, and manganese alloying elements.

Test methods for measuring sensitivity to solidification cracking can be grouped as self-stressing (self – restrained), which uses restraint or stress within the sample to cause cracking, and where external stresses are applied. Self-restrained Houldcroft is one of many self-stressing methods for measuring the susceptibility to solidification cracking of materials [3, 17–19]. The Houldcroft test (also known as the fishbone test) uses a specimen with slots of different depths in a progressive manner. The gas tungsten arc welding (GTAW) process is used to deposit a weld bead. Complete penetration is necessary. Solidification begins as the heat source starts to move inwards from the starting edge of the test sample. Solidification cracking starts from the starting edge and propagates along the centreline. The weld metal is strained in a direction transverse to the welding direction. Cracking of the weld metal occurs because of expansion from the starting edge due to continued heat input to the specimen. The stress along the length of the specimen can be decreased by reducing the width. The susceptibility to cracking is quantified by the crack length from the starting edge [5, 20]. The current investigation was conducted to establish the susceptibility to solidification cracking of the unstabilised, mono- and dual-stabilised ferritic stainless steels using the self-restrained Houldcroft method.

2 Experimental

2.1 Materials

Five (5) experimental alloys (A – E) were produced by Small Alloys and Metallurgical Services (SAMS). Two (2) commercial alloys with one being a dual stabilized (F) and the other dual stabilized containing Mo (G) from Columbus Stainless Ltd, South Africa, were also used. The chemical composition is presented in Table 1. Sample A:0Ti;0Nb is unstabilised, B:0.7Ti is Ti-stabilised, C:0.6Nb is Nb-stabilised, D:0.4Ti;0.6Nb, E:0.4Ti;0.9Nb, and F:0.1Ti;0.4Nb are Ti + Nb stabilised with different elemental contents and G:0.1Ti;0.5Nb;2Mo is dual stabilised containing Mo. The experimental alloy E has a higher Nb content but similar Ti compared to alloy D, and F has lesser Ti and Nb contents.

Table 1 The chemical composition of the ferritic stainless steel alloys

	Composition (mass %)						
Sample	**A:0Ti;0Nb**	**B:0.7Ti**	**C:0.6Nb**	**D:0.4Ti;0.6Nb**	**E:0.4Ti;0.9Nb**	**F:0.1Ti;0.4Nb**	**G:0.1Ti;0.5Nb;2Mo**
Element							
C	0.006	0.006	0.012	0.017	0.011	0.013	0.015
Si	0.6	0.61	0.42	0.4	0.44	0.51	0.53
Mn	0.51	0.5	0.33	0.37	0.37	0.44	0.44
P	0.019	0.018	0.024	0.022	0.025	0.024	0.033
S	0.008	0.007	0.007	0.001	0.004	0.013	0.0033
N	0.069	0.069	0.07	0.069	0.067	0.013	0.0175
Cr	18.03	17.94	18.81	18.12	18.17	17.66	18.10
Nb	0.01	0.003	0.58	0.62	0.92	0.422	0.535
Ti	0.001	0.68	0.03	0.41	0.36	0.146	0.096
Ni	0.23	0.24	0.23	0.35	0.37	0.15	0.16
V	0.007	0.04	0.05	0.11	0.11	0.13	0.13
Cu	0.01	0.02	0.06	0.06	0.07	0.05	0.08
Al	0.2	0.18	0.03	0.02	0.02	0.012	0.014
Mo	0.02	0.02	0.02	0.02	0.02	0.014	2.00
Fe	Bal	Bal	Bal	Bal	Bal	Bal	Bal

Note: Steels A to E are experimental alloys and steels F & G are commercial grades.

2.2 Self-restrained Houldcroft method

The Houldcroft test is not standardized by ASTM as researchers have used different shapes, dimensions and number of slots for their work [5, 20–23]. The dimensions of a Houldcroft sample is given as 76 by 44 mm and have 9 equal slots of 0.8 mm [5, 20, 24]. Samples of 2 mm thickness were wire cut from the alloys A, B, C, D, E, F, and G to dimensions of 90 by 36 mm with each having eight slots of 1 mm (Fig. 1).

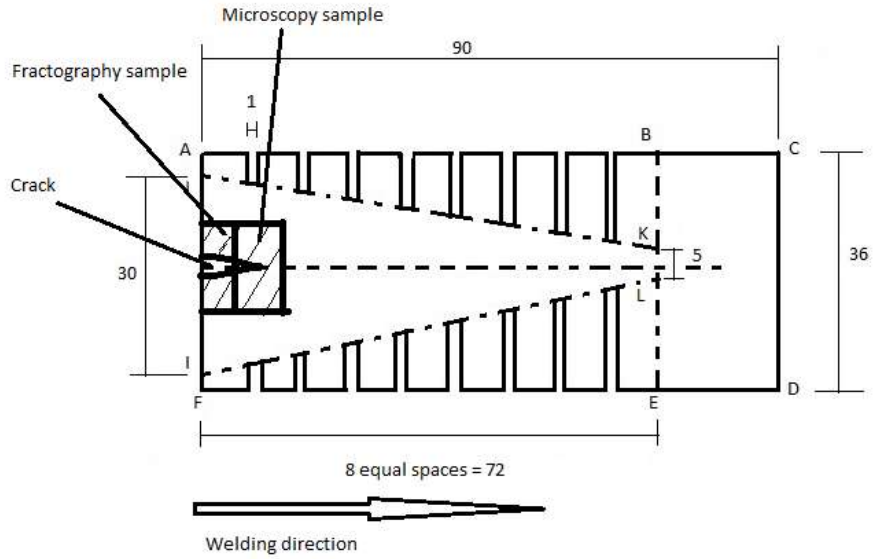

Fig. 1 Dimensions of the modified Houldcroft sample. Sectioning of the sample for microstructural and fractography examination are also shown Automatic autogenous gas tungsten arc welding (GTAW) bead on plate using a Lincoln Electric Square Wave TIG – 355 equipment was employed. The shielding gas was a 99.99% Argon. The welding started on a run-on tab of the same ferritic stainless steel before continuing on the Houldcroft sample. Care was taken to ensure that welding was done in the centre of the Houldcroft specimen. Complete penetration for Houldcroft samples meant different heat inputs was used for the welding speeds of 6 mm/s, 3 mm/s, and 1 mm/s. The welding parameters are presented in Table 2. The average arc efficiency (η) of 0.48 [20] was used to calculate the heat input from equation 1.

$$\text{Heat input} = \frac{\eta VI}{v} \qquad 1$$

where η is the arc efficiency,

V is the welding voltage,

I is the current and

v is the welding speed [20].

Table 2 Houldcroft welding parameters

Speed (mm/s)	**6**	**3**	**1**
Current (A)	250	180 – 190	90 – 120
Voltage (V)	18	15 – 16	12 – 13
Arc length (mm)	2	2	2
Gas flow rate (L/min)	15	15	15
Electrode diameter (mm)	3.2	2.4	2.4
Heat input (kJ/mm)	0.3	0.4 – 0.5	0.5 – 0.8

The repeatability of the self-restrained Houldcroft was tested by evaluating two samples of the same base metal, using the same welding parameters. The samples that cracked, started at the edge of the sample and propagated parallel to the welding direction into a region of lower restraint. A SMZ – 10A stereoscope magnification was

used to mark the crack tip and a Vernier caliper was used to measure the cracked length. The weld bead sizes were measured for any correlation with the solidification crack.

2.3 Microstructure and fractography

The samples were characterized after welding by sectioning close to where the crack occurred (Fig. 1) and where there was no crack, near to the start of the weld. The sectioned pieces were hot mounted in bakelite and polished to a 1 µm surface finish. The polished samples were etched with mixed acids etchant comprising equal parts of nitric acid (HNO_3), hydrochloric acid (HCl) and acetic acid [1]. An XM–15 optical microscope mounted with an Olympus U-TV0.5XC-3 camera was employed for microstructural analysis of the etched samples. A JEOL JSM-IT 300 scanning electron microscope (SEM) with EDX at a voltage of 15 kV which uses Aztec software was used for fractographic studies of the samples. Thermo-Calc version 2015b (TCFE6 database) software was used to determine some of the precipitates through thermodynamic equilibrium and phase diagram calculations using the full chemical composition. Table 3 presents the possible precipitates from the samples used for this study. From Table 3, it can be observed that, the difference between the liquidus and solidus temperatures were similar (40 – 67 K) except the C:0.6Nb steel, which was 110 K. The exception of C:0.6Nb steel having a low solidus temperature of 1660 K might be due to the Nb which forms a eutectic with Fe at 18.6% Nb with the melting point of 1646 K [3, 25]. The eutectic value and the Thermo-Calc value were very similar.

Table 3 Results of Thermo-Calc modelling of the samples

Steel ID	**Liquidus temperature (T_L) (K)**	**Solid state phases in equilibrium with liquid metal**	**Solidus temperature (T_S) (K)**
A:0Ti;0Nb	1773	Ferrite and MnS	1706
B:0.7Ti	1773	Ferrite, TiN, and $Ti_4C_2S_2$	1721
C:0.6Nb	1770	Ferrite, NbC, and MnS	1660
D:0.4Ti;0.6Nb	1773	Ferrite, Ti(C,N), and $Ti_4C_2S_2$	1721
E:0.4Ti;0.9Nb	1773	Ferrite, TiN, and $Ti_4C_2S_2$	1706
F:0.1Ti;0.4Nb	1773	Ferrite, Ti(C,N), and $Ti_4C_2S_2$	1737
G:0.1Ti;0.5Nb;2Mo	1763	Ferrite, Ti(C,N), and $Ti_4C_2S_2$	1723

3 Results

3.1 Cracked length

The top and bottom surface crack lengths were not the same and the average crack length between the two are shown in Table 4. All the ferritic stainless steels cracked during a welding speed of 6 mm/s with varying crack lengths between the different grades (Table 4). The unstabilised ferritic stainless steel did not crack whilst the other grades cracked at a welding speed of 3 mm/s (Table 4). At 1 mm/s welding speed, the Nb stabilised and the dual stabilised steel containing Mo cracked whilst the other alloys did not crack (Table 4). The difference between the average top and average bottom crack lengths are also presented in Table 4. Generally, the top surface crack lengths were longer than the bottom surface crack lengths. Fig. 2 showed a photograph of sample D:0.4Ti;0.6Nb which cracked at the welding speed of 6 mm/s. For the steels characterized, the crack length increased with Ti + Nb content and with welding speed which was more prominent than the stabilization content as circled (Fig. 3). Table 5 shows the weld bead sizes of the top and bottom surface of the alloys. Comparing Tables 4 and 5, there was no relationship between the crack lengths, welding speed and the weld bead sizes.

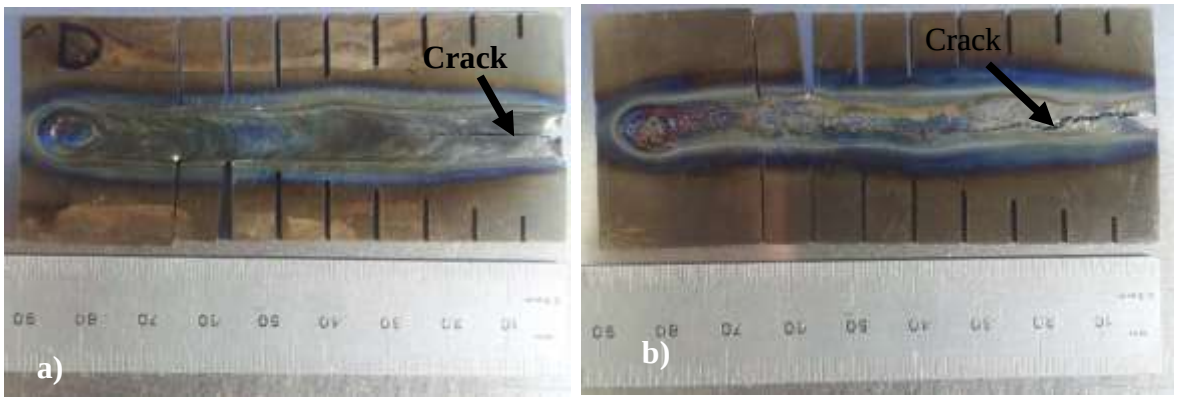

Fig. 2 Photography of cracked sample D:0.4Ti;0.6Nb at a welding speed of 6 mm/s a) top b) bottom

Table 4 The average top and bottom crack lengths (in mm), the difference between the top and bottom surface crack length, as measured using the self-restrained Houldcroft method, as a function of welding speed and steel grade

Steel grade	Average crack length (mm)			Top – bottom surface crack length (mm)		
	6 mm/s	3 mm/s	1 mm/s	6 mm/s	3 mm/s	1 mm/s
A:0Ti;0Nb	5.7	0.0	0.0	0.9	0.0	0.0
B:0.7Ti	25.0	17.8	0.0	1.0	1.3	0.0
C:0.6Nb	34.4	12.3	4.6	1.0	1.0	-0.6
D:0.4Ti;0.6Nb	31.1	15.0	0.0	0.7	3.0	0.0
E:0.4Ti;0.9Nb	32.1	11.3	0.0	-2.4	-0.4	0.0
F:0.1Ti;0.4Nb	26.0	8.5	0.0	2.1	0.9	0.0
G:0.1Ti;0.5Nb;2Mo	4.0	12.2	7.5	-7.9	4.3	5.8

Note: *The negative sign means the bottom surface was longer than the top surface crack length.

Table 5 The weld bead size of the top and bottom surface of the alloys

Alloy	Top (mm)	Bottom (mm)	Top (mm)	Bottom (mm)	Top (mm)	Bottom (mm)
	6 mm/s		3 mm/s		1 mm/s	
A:0Ti;0Nb	6.6	5.2	8.4	6.4	9.5	9.6
B:0.7Ti	6.5	6.1	7.0	8.1	9.0	7.2
C:0.6Nb	9.3	6.5	12.2	10.6	9.0	8.5
D:0.4Ti;0.6Nb	8.6	6.8	9.1	6.7	8.1	7.7
E:0.4Ti;0.9Nb	9.7	6.1	8.5	7.3	8.3	6.8
F:0.1Ti;0.4Nb	7.8	5.2	8.6	6.5	6.2	4.7
G:0.1Ti;0.5Nb;2Mo	8.8	7.4	12.7	9.1	11.0	8.0

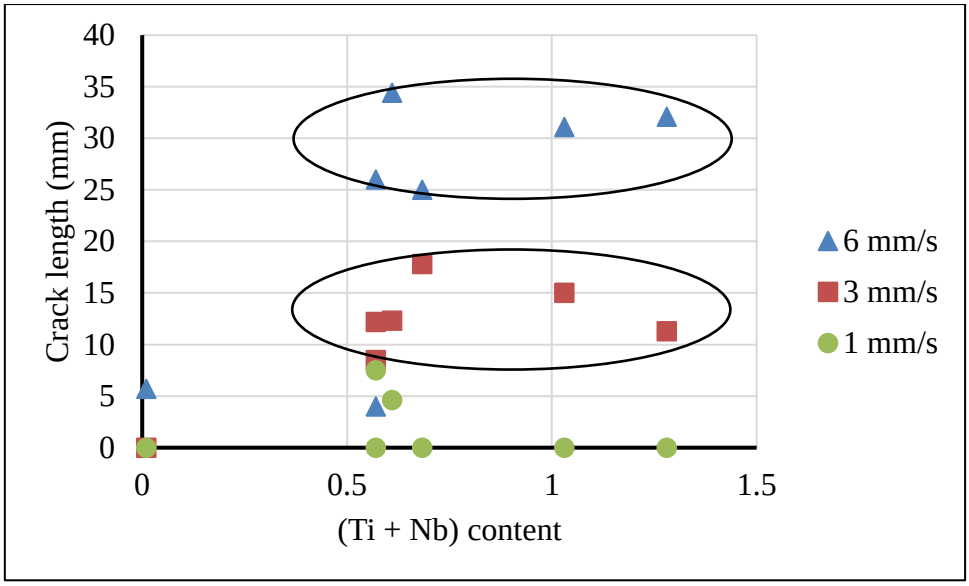

Fig 3 Average crack length against (Ti + Nb) content for a welding speed of 6, 3 and 1 mm/s.

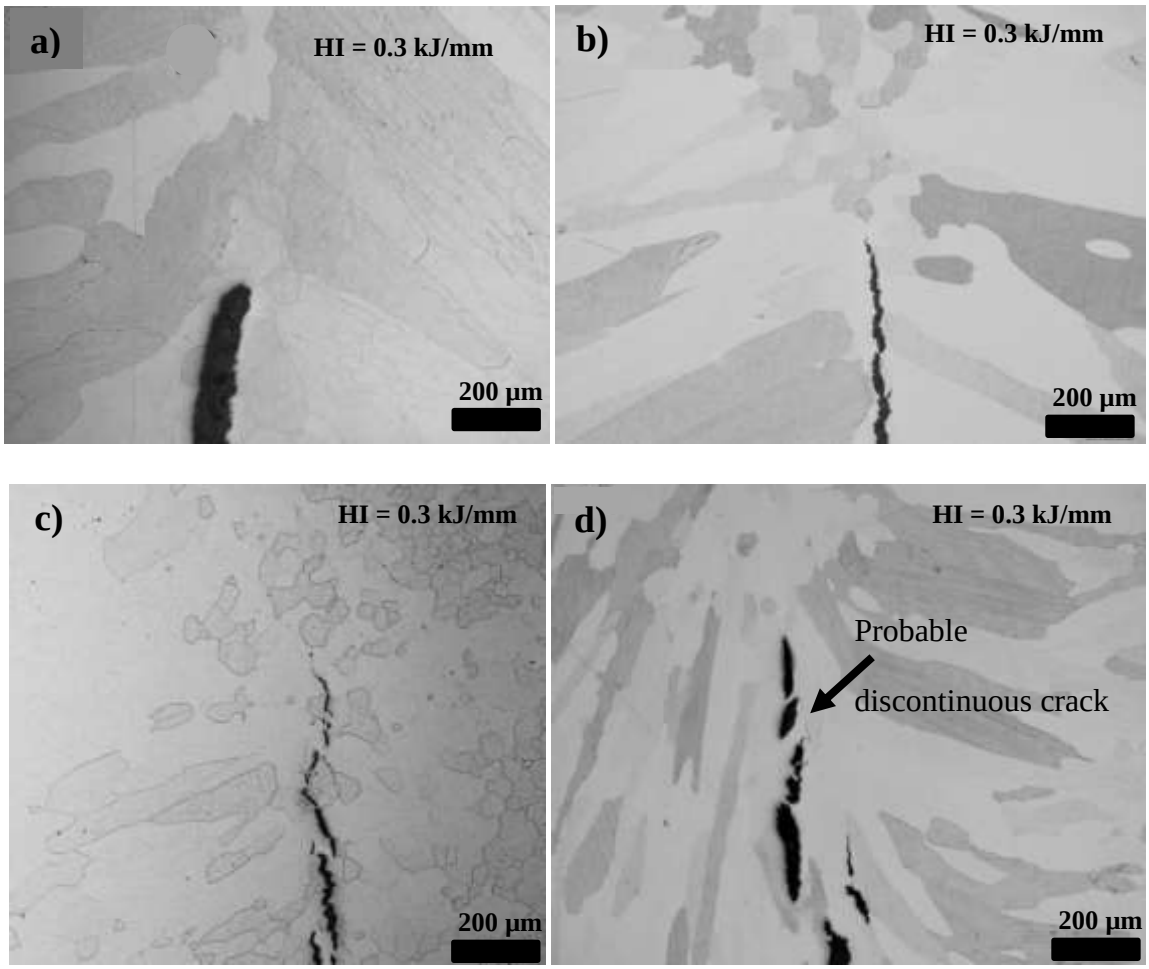

Fig. 4 The crack at the weld showing a) columnar grains of the unstabilized ferritic stainless steel b) columnar grains of the C:0.6Nb – stabilized ferritic stainless steel c) mostly equiaxed grains of the D:0.4Ti;0.6Nb – stabilized ferritic stainless steel d) columnar grains of the F:0.1Ti + 0.4Nb - stabilized ferritic stainless steel, all at a welding speed of 6 mm/s. HI is the heat input

3.2 Microstructure

The unstabilised ferritic stainless steel showed columnar grains which impinged at the weld centreline (Fig. 4a). With the addition of Ti or Nb, there was no change in the grain structure (Fig. 4b). In Fig. 4b, it was observed that there were some equiaxed grains at the crack tip of the C:0.6Nb stabilized alloy. With the addition of dual Ti + Nb stabilization content, the solidification structure was found to contain mostly equiaxed grains in the weld centreline for all dual stabilised steels (Fig. 4c), except for the commercially produced F:0.1Ti;0.4Nb grade (Fig. 4d), which showed columnar grains. Figures 4c & 4d showed that the cracks might be discontinuous. Fig 4c also showed that the crack appeared to pass through an equiaxed grain.

At the welding speed of 3 mm/s, an axial grain which was perpendicular to the weld pool boundary grew between columnar grains in the unstabilised A:0Ti;0Nb alloy (Fig. 5a). This sample did not crack. The mono-stabilised steels and dual stabilised steel containing D:0.4Ti;0.6Nb showed columnar grains adjacent to the weld centreline crack. The dual stabilised steels containing E:0.4Ti;0.9Nb, F:0.1Ti;0.4Nb, and G:0.1Ti;0.5Nb;2Mo showed equiaxed grains next to the crack. The crack in the dual stabilised steels containing E:0.4Ti;0.9Nb, F:0.1Ti;0.4Nb, and G:0.1Ti;0.5Nb;2Mo might be discontinuous (Fig. 5b). At a welding speed of 1 mm/s, the weld metal microstructure consisted of columnar grains (Fig. 5 c & d).

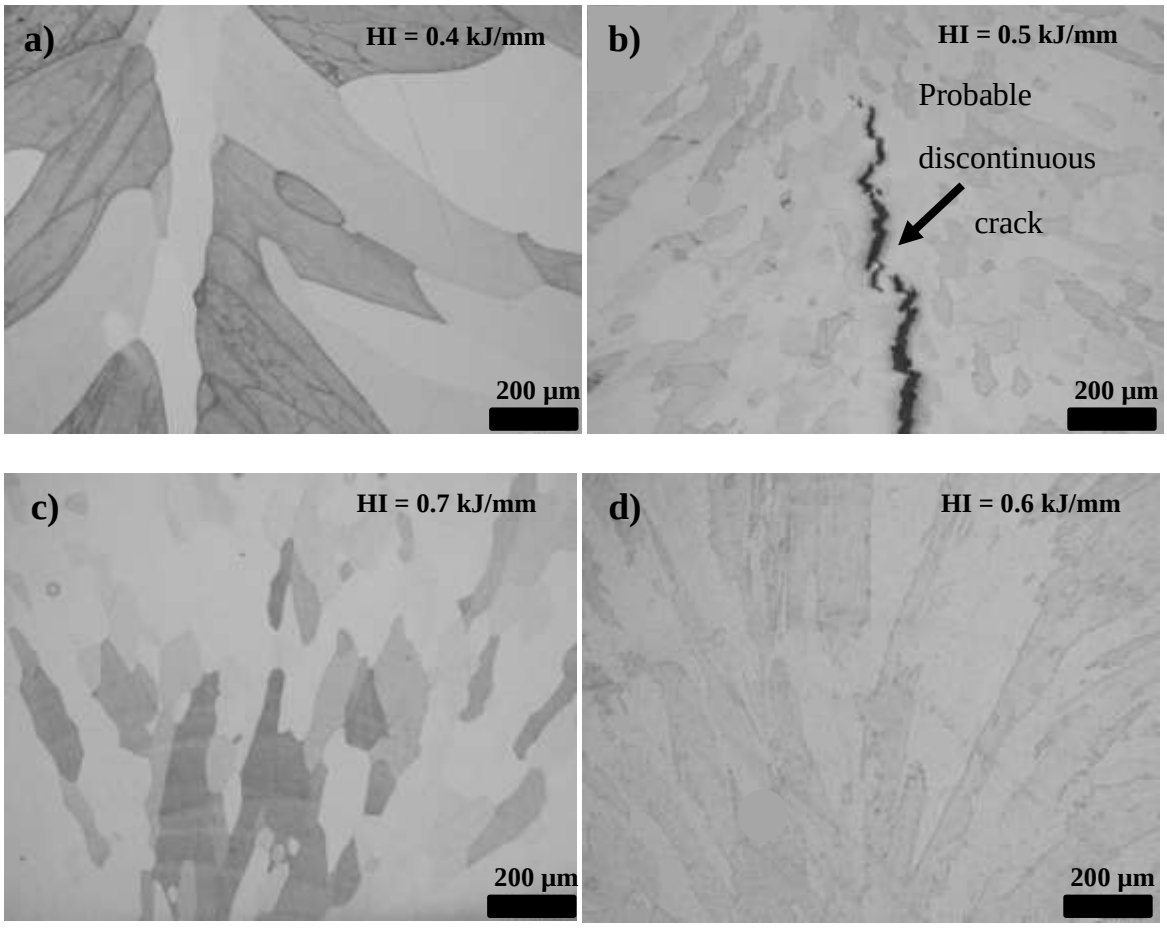

Fig. 5 The microstructure of the weld revealing a) axial grain among columnar grains of the unstabilized (A:0Ti;0Nb) ferritic stainless steel at a welding speed of 3 mm/s b) a crack in the E:0.4Ti;0.9Nb – stabilized ferritic stainless steel at a welding speed of 3 mm/s c) columnar grains of the F:0.1Ti;0.4Nb ferritic stainless steel at a welding speed of 1 mm/s d) columnar grains of the E:0.4Ti;0.9Nb ferritic stainless steel at a welding speed of 1 mm/s

3.3 Fractography

Interdendritic structures were found with all the cracked steels. The steel containing D:0.4Ti;0.6Nb at a welding speed of 6 mm/s showed high fraction eutectic liquid (Fig. 6a) and the rest showed low fraction eutectic liquid (Fig. 6b & 6c) [6]. At a welding speed of 3 mm/s, the steels containing C:0.6Nb and E:0.4Ti;0.9Nb fracture surfaces contained precipitates in the dendrite arms. SEM-EDX semi-quantitative analysis revealed that the

particle of the C:0.6Nb ferritic stainless steel contained mostly Nb and C elements (Fig. 6d). The EDX elemental analysis of the fractured surfaces showed the elements Nb, Ti, O, Mn, Al, Si, Mo, S, and Ni to have contributed to the solidification cracking for all welding speeds (Fig. 6 e&f).

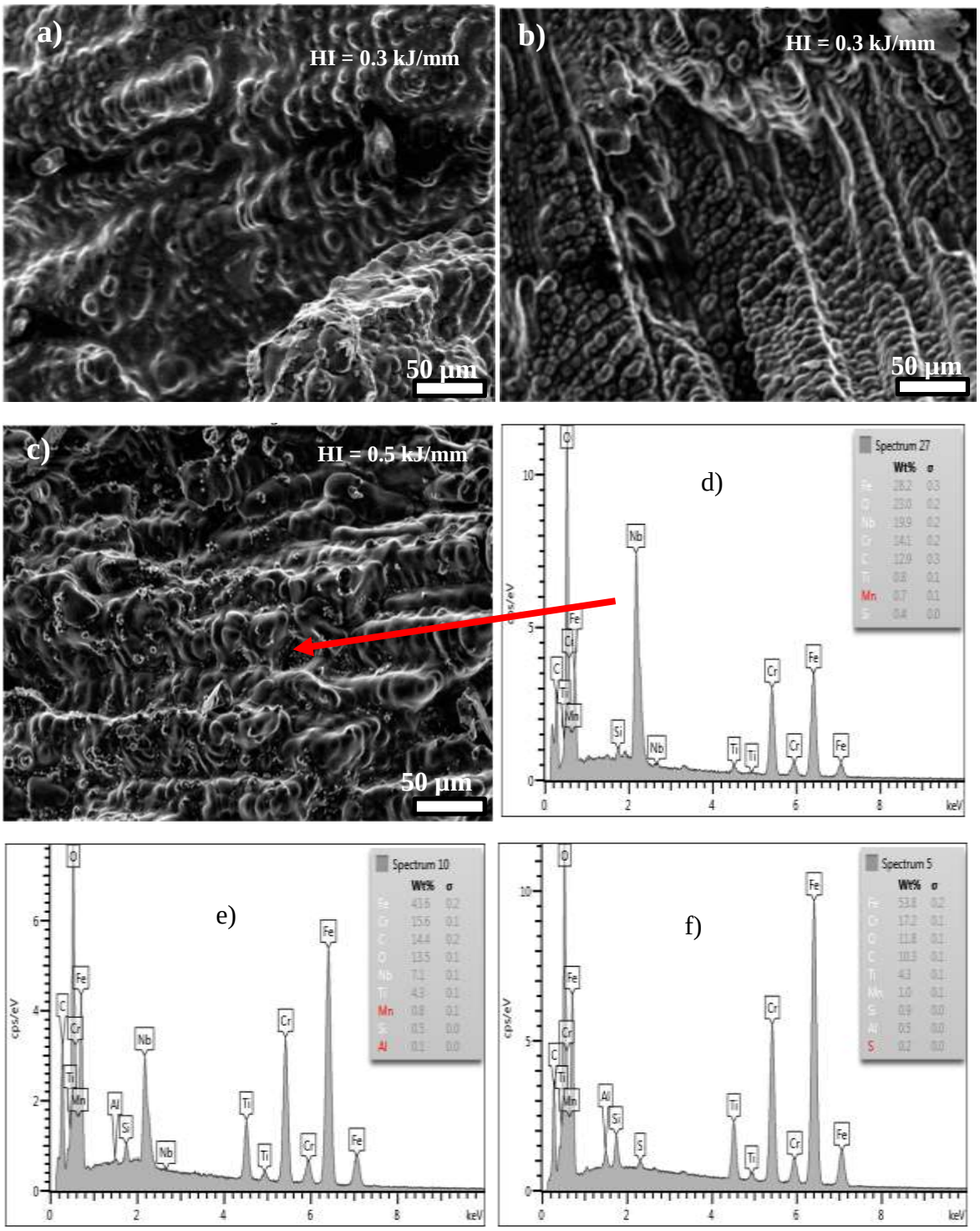

Fig. 6 Secondary electron image of solidification cracking morphology of a) D:0.4Ti + 0.6Nb - stabilized ferritic stainless steel showing high fraction eutectic during welding speed 6 mm/s b) B:0.7Ti - stabilized ferritic stainless steel showing low fraction eutectic during welding speed 6 mm/s and c) C:0.6Nb - stabilized ferritic stainless steel during welding speed 3 mm/s d) EDX spectra of the precipitates in C:0.6Nb - stabilized ferritic stainless steel fracture surface at a welding speed of 3 mm/s e) EDX spectra of the precipitates in D:0.4Ti + 0.6Nb - stabilized ferritic stainless steel fracture surface at a welding speed of 3 mm/s f) EDX spectra of the precipitates in B:0.7Ti - stabilized ferritic stainless steel fracture surface at a welding speed of 6 mm/s

4 Discussion

For the measurement of solidification cracks using Houldcroft method, the crack starts from the starting edge and propagates along the centreline of the weld [5, 17, 20, 24]. All the cracks were observed to have started from the starting edge of the samples and this implied solidification cracking. For the specimens that cracked, there was usually a difference in crack length, as measured on the top and on the bottom surface. This difference was not consistent, with the crack on the top surface sometimes longer, and sometimes shorter, than the crack on the bottom surface. The degree of restraint played a role in the difference between the bottom and top surface crack lengths. The longer lengths might have been caused by greater restraints [5]. This restraint is internal and is caused by the volumetric reduction (shrinkage) during solidification. The properties of the surrounding HAZ and base metal, and the weld bead shape affect the internal restraint [6]. The magnitude of the difference was, in most cases, significantly smaller than the average crack length (Table 4). The difference in the crack length on the top and the bottom surface did not affect the results of this investigation. The weld bead sizes (Table 5) showed no correlation between the alloys, crack lengths and the welding speed. Using the weld bead size influence on strain could not be determined. Literature showed that it is the weld pool geometry that has been used to evaluate solidification cracking [5, 26]. The effect of weld bead shape, concave or convex, can affect solidification cracking in a multipass weld [5]. Measurement of strain is not possible with self-restrained tests which includes the Houldcroft method. The tests developed to measure critical strain rate are 'the variable deformation rate (VDR) test, programmable deformation crack (PVR) test and controlled tensile weldability (CTW) test' [27]. From Table 2, the heat input decreased significantly as the welding speed increased (1 mm/s: 0.5 to 0.8 kJ/mm; 3 mm/s: 0.4 to 0.5 kJ/mm; 6 mm/s: 0.3 kJ/mm). This showed that the risk of solidification cracking increased with a lower heat input. This is in agreement with Ankara and Ari [28].

The unstabilised steel A:0Ti;0Nb cracked at the welding speed of 6 mm/s with the lowest crack length. This might be due to the high welding speed as columnar grains impinged to cause solidification cracking [5-6] (Fig 4a). The steels B:0.7Ti and C:0.6Nb also cracked at this welding speed. Ti forms a low melting eutectic phase at 14% Ti at 1562.15 K and Nb also forms a eutectic with Fe at 18.6% Nb with the melting point at 1646.15 K [3, 25]. The high welding speed and the eutectic phases might have caused the steels B & C to crack. The weld metal of the unstabilised, Ti and Nb stabilised steels revealed columnar grains at a welding speed of 6 mm/s. This is in agreement with literature [5, 6, 20] as high welding speeds produce teardrop weld pool shape which in turn produces columnar grains and are mostly straight.

The resistance to solidification cracking is increased when more grain boundaries per unit volume exist for smaller grains [29]. That is, welds with finer equiaxed grains are less susceptible to solidification cracking [5, 6, 27]. The dual stabilised D:0.4Ti;0.6Nb and E:0.4Ti;0.9Nb steels cracked during the welding speed of 6 mm/s. The dual (Ti + Nb) stabilization showed mostly equiaxed grains in the weld metal and this is contrary to some published literature [5-6, 20]. On the other hand, the presence of equiaxed grains in the weld metal confirmed observations by Villaret et al. [31]. The observed equiaxed grains in the dual (Ti + Nb) stabilized steels could be due to Ti and Nb containing precipitates acting as nucleation sites for equiaxed grains. The solidification crack associated with equiaxed grains does not confirm literature as it has been stated that equiaxed grains resist solidification cracking [5, 6, 26-27]. The crack in the equiaxed grains showed that neither equiaxed nor columnar grains could resist the propagation of solidification cracks in the Houldcroft samples [6]. The crack which seemed to pass through an equiaxed grain (Fig 4c) was considered not to be representative of the microstructures, given that the SEM image (Fig.6a) showed the crack path to be intergranular. This crack was observed at the tip of the whole crack length. From Fig 1, the experimental diagram for analysis for fractography was such that, such investigations were not conducted at the crack tip to confirm this fracture through the grains.

The commercial F:0.1Ti;0.4Nb steel revealed columnar grains with the crack adjacent to the weld centreline. The columnar grains might be due to the low Ti + Nb content as the high content produced equiaxed grains. Villaret et al. [31] reported that columnar grains of ferritic stainless steel changed their structure to equiaxed grains for contents above 0.15 wt% Ti.

At the welding speed of 3 mm/s, the unstabilised A:0Ti;0Nb alloy showed an axial grain. The axial grain might be due to it initiating from the fusion boundary from the start of the weld and continuing along the weld length, thereby blocking the columnar grains from impinging [5-6]. This might have contributed to steel A:0Ti;0Nb being resistant to solidification cracking. The zero stabilization of Ti and Nb in ferritic stainless steels also contributed to the resistance of steel A:0Ti;0Nb to solidification cracking [1]. The other steels (steels B to G) cracked during the welding speed of 3 mm/s. The high welding speed [5-6] and the Ti and Nb stabilization contents [1] were a contributory factor to the susceptibility of solidification cracking of these steels.

Columnar grains were seen in the weld metal at the welding speed of 1 mm/s, During low welding speed, the weld pool shape is elliptical and this caused the trailing boundary to be curved, thereby making the columnar grains to grow perpendicular to the pool boundary [27, 29]. Low welding speeds are not susceptible to solidification cracking due to the columnar grains which do not impinge [6]. That might have contributed to the steels A, B, D, E and F not cracking. The steels C and G cracked and this might be due to the Nb content of above 0.5 wt% in these steels.

The interdendritic structures found with all the cracked steels implied solidification cracking. The low fraction eutectic has been found to have a relatively low fraction (<5%) of eutectic liquid and the fracture surface reveals a very clear dendritic structure. The fracture surface of high fraction eutectic liquid, on the other hand, is obscured by the backfilling liquid. This liquid coats the dendrites and has been shown to be about 10% eutectic liquid [6]. Some of the steels at a welding speed of 3 mm/s were found to contain precipitates in the dendrite arms. From the literature, such precipitates are considered to contribute to solidification cracking (Fig. 6c), For example, Lippold [6] reported the presence of second phase particles on the fracture surface of a Nb-bearing Ni-base alloy due to eutectic reaction. As solidification began, the solute elements were rejected from the liquid into the mushy zone. At the later stage of solidification, the rejected elements acted as impurities to weaken the boundary layer, thereby resulting in cracking along the grain boundary. Nb has also been found to form eutectics [3]. The C:0.6Nb ferritic stainless steel contained mostly Nb and C elements. This particle was likely to be a NbC precipitate as the Thermo-Calc simulations predicted a NbC to be a precipitate from the C:0.6Nb alloy (Table 3).

The EDX elemental analysis of the fractured surfaces showed the elements Nb, Ti, O, Mn, Al, Si, Mo, S, and Ni to have contributed to the solidification cracking for all welding speeds. These elements were seen as being ejected to the grain boundary during solidification to form impurities which eventually caused the solidification cracking.

4 Conclusions

The seven alloys investigated to ascertain the susceptibility to solidification cracking of the ferritic stainless steel revealed the following:

1. The unstabilised ferritic stainless steel can be said to be resistant to solidification cracking. The addition of Ti slightly increased the susceptibility to solidification cracking, as the samples cracked in welding speeds 6 mm/s and 3 mm/s. The addition of Nb to the ferritic stainless steel resulted in a significant increase in the susceptibility to solidification cracking as there was cracking at all three welding speeds of 6 mm/s, 3 mm/s, and 1 mm/s. The addition of Ti and Nb to the ferritic stainless steels increased the length of the solidification crack.

2. The solidification structure of the unstabilised (A:0Ti;0Nb), B:0.7Ti and C:0.6Nb stabilised and the commercial dual (F:0.1Ti;0.4Nb) stabilised ferritic stainless steels revealed columnar grains. The experimental dual stabilised ferritic stainless steels (D:0.4Ti;0.6Nb & E:0.4Ti;0.9Nb) showed mostly equiaxed grains at a welding speed of 6 mm/s. The dual stabilised plus Mo (G:0.1Ti;0.5Nb;2Mo) alloy showed equiaxed grains in the weld region for speeds 6 and 3 mm/s. It seems that the weld solidification structure does not contribute to the susceptibility to cracking as both columnar and equiaxed grains cracked in ferritic stainless steels.
3. Elemental analysis revealed Nb, Ti, O, Mn, Al, Si, Mo, S, and Ni as associated with the fractured surfaces of all the alloys in all the welding speeds.

5 Acknowledgement

The authors want to thank Office of Research, Innovation, and Development (ORID), University of Ghana, Department of Research and Innovation Support (DRIS), and Department of Welding Engineering, both of University of Pretoria for financial assistance.

References

[1] Lippold JC, Kotecki DJ (2005) Welding metallurgy and weldability of stainless steels, 1st edn. New Jersey: John Wiley and Sons..

[2] Mohandas T, Madhusudhan RG, Naveed M (1999) A comparative evaluation of gas tungsten and shielded metal arc welds of a ferritic stainless steel. J. Mater. Process. Technol 94(2–3):133–140.

[3] Folkhard E (1988) Welding metallurgy of stainless steels, 1st edn. Vienna: Springer Vienna.

[4] Gordon W, van Bennekom A (1996) Review of stabilisation of ferritic stainless steels," Mater. Sci. Technol 12:126–131.

[5] Kou S (2003) Welding metallurgy, 2_{nd} edn. New Jersey: John Wiley & Sons.

[6] Lippold JC (2015) Welding metallurgy and weldability, 1st edn. Hoboken, New Jersey: John Wiley & Sons.

[7] Aggen G, Akstens FW, Allen CM, Avery HS (1993) ASM handbook volume 1. United States of America: ASM International.

[8] Nelson DE, Baeslack III WA, Lippold JC (1987) An investigation of weld hot cracking in duplex stainless steels Weld. J 66(8):241s–250s.

[9] Nunes RM, Alia BL, Alley RL, Apblett Jr. WR, Baeslack III WA, Etc. (1993) ASM handbook volume 6 welding, brazing and soldering. USA: ASM International..

[10] Slyvinsky et al (2005) Influence of welding speed on the hot cracking resistance of the nickel-base alloy NiCr25FeAlY during TIG-welding, Book: Hot Cracking Phenomena in Welds, Berlin Heidelberg: Springer Berlin Heidelberg, :42–58.

[11] Shankar V, Gill TPS, Mannan SL, Sundaresan S (2003) Solidification cracking in austenitic stainless steel welds. Sadhana 28(3–4):359–382.

[12] Sun Z. (1992) A study of solidification crack susceptibility using the solidification cycle hot-tension test. Mater. Sci. Eng. A 154:85–92.

[13] Varol I, Baeslack III WA, Lippold JC (1989) Characterization of weld solidification cracking in a duplex stainless steel. Metallography 23:1–19.

[14] Lakshminarayanan AK, Shanmugam K, Balasubramanian V (2009) Effect of welding process on tensile and impact properties, hardness and microstructure of ferritic stainless steel by duplex stainless steel filler metal. J. Iron Steel Res. Int 16(5):66–72.

[15] Lakshminarayanan A, Shanmugam K, Balasubramanian V (2009) Effect of autogenous arc welding processes on tensile and impact properties of ferritic stainless steel joints, J. Iron Steel Res. Int 16(1):62–16.

[16] Kah DH, Dickinson DW (1981) Weldability of ferritic stainless steels. Weld. J. 64(16):135-s–142-s.

[17] Campbell RD, Walsh DW (1993) Weldability testing in ASM handbook volume 6 :603–613

[18] Lundin CD, Delong WT Spond DF (1976) The fissure bend test," Weld. J. 55(6):145–151.

[19] Srinivasan G, Divya M, Das CR, Albert SK, Bhaduri AK, Lauf S, Stubenrauch S, lenk A (2015) Weldability studies on borated stainless steel using Varestraint and Gleeble test. Weld World 59:119–126.

[20] Lancaster JF (1999) Metallurgy of welding, 6th edn. Abington, Cambridge England: Woodhead Publishing Limited.

[21] Madhusudhan RG, Mukhopadhyay AK, Sambasiva Rao A (2005) Influence of scandium on weldability of 7010 aluminium alloy, Sci. Technol. Weld. Join 10(4):432–441.

[22] Adamiec J (2011) The influence of construction factors in the weldability of AZ91E alloy, Arch. Metall. Mater 56(3):769–778

[23] Safari AR, Forouzan MR, Shamanian M (2012) Hot cracking in stainless steel 310s, numerical study and experimental verification, Comput. Mater. Sci 63:182–190.

[24] Krysiak KF, Grubb JF, Pollard B, Campbell RD (1993) Selection of wrought ferritic stainless steels in ASM handbook, volume 6: welding, brazing, and soldering :443–455. [25] R. M. Notis, N. A. Gjostein, N. C. Jessen Jr., E. C. Kendall, and Etc, *ASM Handbook Volume 3 Alloys Phase Diagrams*. 1992.

[26] Wolf M, Schobbert H, Böllinghaus T (2005) Influence of the weld pool geometry on solidification crack Formation. Book: Hot Cracking Phenomena in Welds, Berlin Heidelberg: Springer Berlin Heidelberg, :245–270.

[27] Cross CE, Coniglio N (2008) Weld solidification cracking: critical conditions for crack initiation and growth, Book: Hot Cracking Phenomena in Welds II, Berlin Heidelberg: Springer Berlin Heidelberg, :39–58.

[28] Ankara A, Ari HB (1997) Determination of hot crack susceptibility of various kinds of steels, Mater Des. 17(5):261–265.

[29] Cross CE (2005) On the origin of weld solidification cracking, Book: Hot Cracking Phenomena in Welds, Berlin Heidelberg: Springer Berlin Heidelberg, :3-18.

[30] Kou S (2003) Solidification and liquation cracking issues in welding," JOM, :37–42.

[31] Villaret V, Des chaux-Beaume F, Bordreuil C, Fras G, Chovet C, Petit B, Faivre L (2013) Characterization of gas metal arc welding welds obtained with new high Cr–Mo ferritic stainless steel filler wires, Mater. Des 51:474–483.

[32] DuPont JN (2011) Fundamentals of weld solidification, in ASM handbook volume 6, welding, brazing and soldering, USA: ASM International :96–114.